RESEARCH

Possibility for detecting 14 typical odorants occurring in drinking water by employing human odor-binding protein OBP2a

Xinying Chang[1,2], Fuguo Qiu[1], Chunmiao Wang[2,3,4*], Yaohan Qian[2,3], Yongxin Zhang[1,2], Qingyuan Guo[5], Qi Wang[2,3,4], Shihao Wang[6], Min Yang[2,3,4] and Jianwei Yu[2,3,4*]

Abstract

Odor issues occurring in drinking water have been a big challenge to face for water suppliers globally, which highly commend to develop quick or on-site odor detection tools for the management of odor problems. Olfactory sensors based on odor-binding proteins (OBPs) have been utilized to analyze pollutants in food and air samples, while their application for the detection of typical odor-causing compounds in drinking water is rarely reported, partly due to the lack of knowledge about the binding properties of odorants. In this study, the binding affinity and mechanism of human odor-binding protein OBP2a to 14 typical odorants in water were first assessed using fluorescent competitive binding assays and molecular docking techniques. The 14 odorants include 7 aldehydes, 2 terpenes, 2 thioethers, bis(2-chloro-1-methylethyl) ether (DCIP), 2-ethyl-4-methyl-1,3-dioxolane (2E4MDL), and 2-isobutyl-3-methoxypyrazine (IBMP). The results showed that OBP2a could bind to 9 odorants (K_i = 29.91 μmol/L–48.36 μmol/L), including IBMP, 2-MIB, and six aldehydes (hexanal, heptanal, benzaldehyde, 2-octenal, decanal, and β-cyclocitral), among which stronger binding affinity for aldehydes is observed (K_i = 29.91 μmol/L–43.87 μmol/L). Molecular docking confirmed that Lys112 and Phe97 are major amino acid residues involved in the binding of the most target odorants. To be specific, IBMP and aldehydes can form hydrogen bonds with Lys112; aromatic ring-containing odorants such as IBMP and benzaldehyde can also form pi–pi stacking with Phe97. The binding affinity of OBP2a to fatty aldehydes including hexanal, heptanal, 2-octenal, decanal, and β-cyclocitral increased with the increase of hydrophobicity of aldehydes. The valuable information to the binding of OBP2a to typical odorants in this study would provide a theoretical foundation for the development of OBP-based odor detection biosensors to achieve quick detection in drinking water, further helping the improvement of water treatment processes in the water industry.

Highlights

- OBP2a has a broad binding spectrum and binds preferentially to aldehydes
- Lys112 and Phe97 are main amino acid residues involved in binding of 14 odorants
- Hydrogen bond contributes to the compact binding of OBP2a and aldehydes
- Hydrophobicity of aldehydes affects significantly their binding affinity to OBP2a

*Correspondence:
Chunmiao Wang
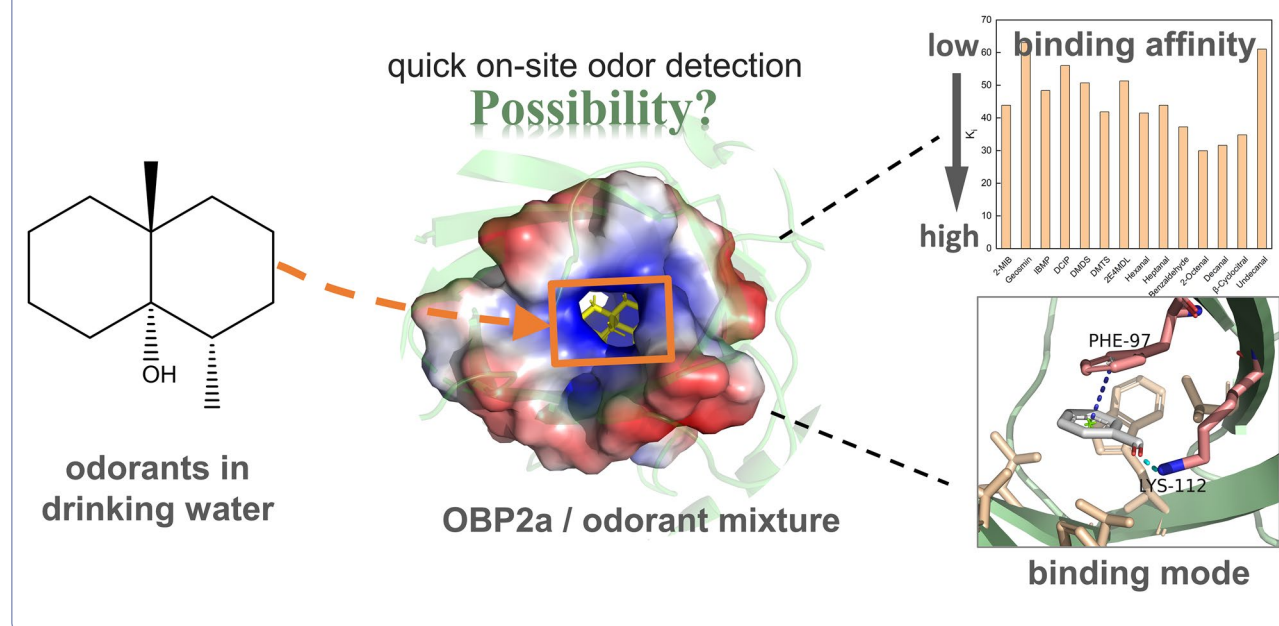cmwang@rcees.ac.cn
Jianwei Yu
jwyu@rcees.ac.cn
Full list of author information is available at the end of the article

Chang *et al. Environmental Sciences Europe*   (2023) 35:44

Page 2 of 12

Graphical Abstract

Introduction

Taste and odor, as an important esthetic indicator of drinking water, has become an essential factor that affects consumers' judge on water quality and safety [1–3]. Water utilities have to face a big challenge or difficulty to cope with taste and odor problems in drinking water worldwide [4, 5]. In China, serious water supply crisis due to offensive odors occurred in Wuxi City in 2007 [1, 6] and Lanzhou City in 2014 [7]. Moreover, a national investigation across China showed that 80% of the sampled surface source waters exhibited some odor issues, including swampy/septic, earthy/musty, fishy and chemical odors [8, 9].

It is reported that numerous odorants with different physio-chemical properties have been identified to cause odor problems in drinking water [5]. 2-Methylisoborneol (2-MIB) and geosmin (GSM), the main earthy/musty odorants in China, have odor thresholds of 10 ng/L and 4 ng/L, respectively [10]. Pyrazines can also contribute to earthy/musty odors in drinking water at low ng/L level [11]. Thioethers including dimethyl disulfide (DMDS) and dimethyl trisulfide (DMTS), the major cause of swampy/septic odor in water crisis of Wuxi City (2007), have odor thresholds of 10 ng/L and 30 ng/L, respectively [1]. Some aldehydes could cause grassy or fishy

odor problems at concentrations of hundreds of ng/L–μg/L [12, 13]. Bis(2-chloro-1-methylethyl) ether (DCIP) and 2-ethyl-4-methyl-1,3-dioxolane (2E4MDL) exhibit chemical, solvent-like odors at ng/L level [4]. 2E4MDL has been involved in several serious odor incidents worldwide [4]. These odorants are frequently detected in source water, and some of which (e.g., 2-MIB, DCIP) were also present in the corresponding finished water with concentrations up to hundreds of ng/L [5]. To prevent the public from exposure to odor in drinking water, the newly issued *Standards for Drinking Water Quality* of China (GB5749-2022) regulate a limit of 10 ng/L for the earthy/musty odorants 2-MIB and geosmin, and a guideline of 30 ng/L for swampy/septic odorants DMDS and DMTS in appendix A. The widespread occurrence of odor problems in drinking water, low odor thresholds, as well as the requirements of odorless water from standards, highlight a growing need to develop rapid or on-site odorant detection tools for quick response to employ applicable measures or management strategies to cope with taste and odor problems in drinking water industry.

In general, the instruments of gas chromatography–mass spectrometry (GC–MS) or gas chromatography–triple quadrupole tandem mass spectrometry (GC–MS/MS) were employed for the simultaneous quantification

Chang *et al. Environmental Sciences Europe*   (2023) 35:44

Page 3 of 12

of various odorants in water [5, 14]. However, these methods usually need complex pre-treatment and expensive instruments, which make impossible for quick or on-site detection [15, 16]. In recent years, with the continuous exploration and recognition on olfactory system and odor perception mechanism [17–19], some bionic olfactory biosensors have been successfully developed by adopting biomaterials to detect various odorants in different environments [20–23]. Compared to the biomaterials of olfactory tissues, olfactory cells and olfactory receptors, odor-binding proteins (OBPs) were thought to be good candidates due to their excellent biological stability and the broad binding spectrum [20, 24]. Specifically, odor-binding proteins from organisms such as pigs, cattle, and rats have been reported for the detection of ligands including octenol, carvone, and alcohol with detection limits down to femtomolar levels [23, 25–27].

For the olfactory perception, OBPs are thought to play a mediating role by providing hydrophobic pockets that bind odor molecules and transport them to olfactory receptors [24]. OBPs are abundantly expressed in the mucus of various species and can be divided into insect OBPs and mammalian OBPs [28], of which, two related OBPs have been identified in humans: OBP2a and OBP2b [28, 29]. OBP2a is mainly expressed in the nasal epithelium, lacrimal glands, and salivary glands, while OBP2b is expressed in the prostate and mammary glands [29]. Not only have they been identified as relevant transporter proteins in olfactory recognition, but they can also act as scavengers to neutralize toxic volatiles or to prevent saturation of odor receptors [30]. Previous studies have shown that OBP2a has a strong affinity for medium and long-chain fatty acids and aldehydes, and has been adopted for biosensor development [31, 32]. In contrast, the application of OBP2a for the detection of typical odorants in drinking water was limited, partly due to the lack of knowledge about the binding properties with odorants. It would be essential to assess the binding capacity and mechanism with OBPs for further development of biosensors to detect odorants.

In the present study, 14 typical odorants in drinking water were selected to assess the binding characteristics and mechanism with human odor-binding protein OBP2a. The 14 odorants include seven aldehydes, two terpenoids, two thioethers, bis(2-chloro-1-methylethyl) ether, 2-ethyl-4-methyl-1,3-dioxolane, and 2-Isobutyl-3-methoxy pyrazine (IBMP), which are either frequently detected in raw and finished drinking water, or involved in some odor incidents previously. Fluorescence competitive binding assay was employed to determine and screen the odorants with good binding capacity to OBP2a. Then by using molecular docking, the binding modes and mechanism of OBP2a to these odorants were

first characterized. This study provides a theoretical basis for further development of olfactory protein-based biosensors for monitoring and early warning of odor issues, which will benefit the odor problem control and management in water industry.

Materials and methods

Chemicals and reagents

All odorant standards were obtained from Beijing Ruizhihanxing Technology Co. (China) at a minimum purity of 95% (most > 99%, see catalogue numbers and brand names of standards in Additional file 1: Table S1). Chromatographic-grade methanol was obtained from Fisher Scientific Co. (China). The fluorescent probes including N-phenyl-1-naphthylamine (1-NPN), 1-aminoanthracene (1-AMA) and 8-anilino-1-naphthalene sulfonic acid (ANS) were bought from Sigma-Aldrich Co. (USA) (purity > 97%). The fluorescent probes and all odorant standards were dissolved in methanol for a 1 mmol/L stock solution. Bicinchoninic acid assay (BCA) protein assay kit and phosphate buffered solution (PBS) of pH = 7.4, were purchased from Beijing Solarbio Science & technology Co. Ltd (China). Ultrapure deionized water (> 18 MΩ cm) was produced with a Milli-Q purification system. The detailed information for the 14 odorants is shown in Table 1.
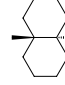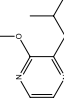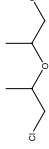
Expression and purification of OBP2a
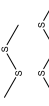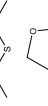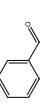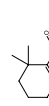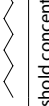
The expression and purification of the active recombinant OBP2a was cloned from the full-length cDNA of humans in Cellregen Biotech Co., Ltd (China). Briefly, a DNA sequence encoding the OBP2a was cloned into the expression vector pET30a (+), transferred into E. coli BL21 (DE3) cells and expressed at 37 °C with induction of IPTG [33]. Harvested host cells are sonicated and centrifuged to obtain supernatant, which were purified by Ni affinity chromatography. Next, the molecular mass of recombinant OBP2a was determined to be 19 kDa by sodium dodecyl sulfate—polyacrylamide gel electrophoresis (SDS-PAGE) analysis (Additional file 1: Fig. S1). The concentration of recombinant OBP2a was determined to be 400 μg/mL by BCA, which was further dispensed into 1.5-mL Eppendorf tubes in a buffer of $NaHCO_3$ (20 mM, pH 8.3) and stored at −20 °C.

Fluorescent competitive binding assays

Fluorescence competitive binding assays were performed on a fluorescence spectrophotometer F-7000 (Hitachi, Japan) in a 1-cm light path quartz cuvette. The slit widths used for excitation and emission were 10 nm.

Fluorescent probes including 1-NPN, 1-AMA, and ANS were tested for binding OBP2a and the procedure was as follows: OBP2a, fluorescent probe and a mixture

Table 1 The detailed information for the 14 odorants [5, 12]

Odorants		Abbreviations	Structures	CAS	MW [a]	LogK$_{ow}$ [b]	OTC [c] (µg/L)	Odor descriptors	Concentrations in finished water (ng/L)	Detection frequency (%)
Terpene	2-Methylisoborneol	2-MIB		2371–42-8	168.18	3.31	0.010	Musty/earthy	n.d.-576	36
	Geosmin	GSM		19700–21-1	182.30	3.57	0.004	Musty/earthy	n.d.-10	50
Pyrazine	2-Isobutyl-3-methoxy pyrazine	IBMP		24683–00-9	166.22	2.86	0.002	Musty/earthy	n.d.-0.02	2.2
Ether	Bis(2-Chloro-1-methylethyl) ether	DCIP		108–60-1	171.07	1.47	0.197	Chemical/solvent-like	n.d.-1191	36
Thioether	Dimethyl disulfide	DMDS		624–92-0	94.20	1.87	0.030	Swampy/septic	n.d.-8.7	45
	Dimethyl trisulfide	DMTS		3658–80-8	126.25	1.87	0.010	Swampy/septic	n.d.-3.3	25
Cyclic acetal	2-Ethyl-4-methyl-1,3-diox-olane	2E4MDL		4359–46-0	116.16	1.02	0.005 – 0.884	Solvent-like/sweet	n.d.-40.5	11
Aldehyde	Hexanal	–		66–25-1	100.16	1.80	0.3 – 14	Grassy/fatty	n.d.-243	79
	Heptanal	–		111–71-7	114.19	2.29	3	Fishy/fatty	n.d.-578	42
	Benzaldehyde	–		100–52-7	106.12	1.71	4.5	Bitter almond	n.d.-592	92
	2-Octenal	–		2548–87-0	126.20	2.57	3	Fishy	n.d.-34.5	1.4
	Decanal	–		112–31-2	156.26	3.76	0.8	Fruity	n.d.-153	35
	β-Cyclocitral	–		432–25-7	152.23	3.44	19.3	Grassy/sweet-tobacco	n.d.-57.4	32
	Undecanal	–		112–44-7	170.29	4.25	0.55	Fatty/fruity	800	–

[a] Molecular weight; [b] octanol–water partition coefficient; [c] odor threshold concentration

Chang *et al. Environmental Sciences Europe*   (2023) 35:44

Page 5 of 12

of the two with equal masses (2 μmol/L) were scanned at an excitation wavelength of 290 nm to verify an interaction between the two. Then, a 2 μmol/L solution of recombinant protein in 100 mmol/L PBS, pH 7.4, was titrated with aliquots of 1 mmol/L fluorescent probe solutions in 2 μL increments, resulting in a final concentration of 2–20 μmol/L. The OBP2a/1-NPN, OBP2a/1-AMA and OBP2a/ANS mixture were excited at 337 nm, 256 nm and 378 nm, respectively, and the corresponding emission spectra are 350–600 nm, 270–550 nm, and 380–600 nm, respectively. The maximum saturation fluorescence intensity was determined by a non-linear regression between fluorescent probe concentration and the corresponding maximum fluorescence intensity using GraphPad Prism 7.0 software. The fitting model is "one-site specific binding", assuming that the protein is 100% active and the binding stoichiometry in the saturated state is 1:1 (protein: ligand). The binding constant of OBP2a to the fluorescent probe was calculated using Scatchard equation: $B/F = (B_{max}/K_d) - (B/K_d)$, where B is the concentration of receptor-ligand specific binding, F is the free ligand concentration, K_d is the binding constant and B_{max} is the maximum saturation concentration of ligand binding (the total amount of receptor).

The binding constant of each fluorescent probe was calculated, and one with lower binding constant was selected to measure the binding affinity of OBP2a to 14 odorants. A mixture of equal masses of OBP2a and probe (2 μmol/L) was prepared for the assessment of binding properties of odorants, and the mixture was left to stand for two minutes prior to the determination of the maximum fluorescence intensity. For each odorant, 15 concentration levels (5–75 μmol/L) with each level differing 5 μmol/L were fully reacted and the maximum fluorescence intensity was recorded for each gradient. Three replicates were performed for each odorant. The dissociation constant of OBP2a to each odorant was calculated using the equation: $K_i = IC_{50}/(1 + [probe]/K_d)$, where [probe] is the free concentration of fluorescent probe, K_d is the binding constant of OBP2a to fluorescent probe and IC_{50} is the concentration of ligand added when the fluorescence intensity is reduced by half, which was calculated using non-linear regression (log [inhibitor] vs. normalized response, variable slope) (GraphPad Prism v.7.0).

Molecular docking

The three-dimensional structure of OBP2a with two mutations (99, from Cys to Ser; 112, from Lys to Asn) was downloaded from Protein Data Bank (http://www.rcsb.org) [34] as described by Arne Skerra et al. [29] (PDB entry code, 4run). Pymol software is utilized to prepare OBP2a structure without above amino acid site mutation for molecular docking analysis.

Schrödinger-Maestro v11.9, a protein preparation wizard was used to prepare and refined the OBP2a structure. The predicted protein was pre-processed as follows: bond order and charges are redistributed; missing hydrogen atoms are added and co-crystallized water molecules are removed. The pre-processed protein was optimized and minimized using the force field OPLS3e with the maximum heavy atom root-mean-square deviation to 0.30 Å [35].

The 2D structure of 14 odorants (ligands) was retrieved from PubChem online database (https://pubchem.ncbi.nlm.nih.gov/) [36]. The LigPrep tool embedded in Maestro was used to further prepare the minimized 3D structure. Force field OPLS3e is used to minimize ligand energy [37–39]. Complete stereoisomers at most 32 per ligand were generated by retaining specified chiralities in the desalting process.

The Deep Site, an online server for protein binding site prediction, was used to determine the active sites of the OBP2a. The docking was performed in Extra Precision mode (XP). Different docking scores were obtained by computing the synthetic effects of electrostatic forces, van der Waals forces, hydrophobic interactions, hydrogen bonds, and other non-covalent bonds [40, 41] as well as antagonistic effects with amino acid residues. Ten different poses were considered for each ligand, and the best pose was selected based on interaction mode and docking score to evaluate the binding affinity between OBP2a and odorant.

Results and discussion

Characterization of the binding of OBP2a to 1-NPN

The fluorescence spectra of OBP2a, probes (1-NPN, 1-AMA, ANS), and a mixture of equal amounts of OBP2a and one probe at an excitation wavelength of 290 nm are shown in Fig. 1 and Additional file 1: Fig. S2. The maximum emission wavelength of OBP2a were 328 nm (line a). The maximum emission wavelengths of 1-NPN, 1-AMA and ANS were 425 nm, 527 nm, and 479 nm (line b), respectively. The fluorescence intensity of OBP2a decreased and fluorescence burst occurred after mixing OBP2a and probes, and the fluorescence maximum emission peak of probes was blue-shifted (line c), indicating that there was an interaction between OBP2a and the probes, and an energy transfer occurred [42].

The binding curves of OBP2a with 1-NPN, 1-AMA and ANS are shown in Fig. 2 and Additional file 1: Fig. S2. Compared to 1-AMA and ANS, 2 μmol/L 1-NPN could generate a relative strong fluorescent signal (fluorescent intensity of 1474); the fluorescence intensity rapidly increased with the addition of 1-NPN and reached
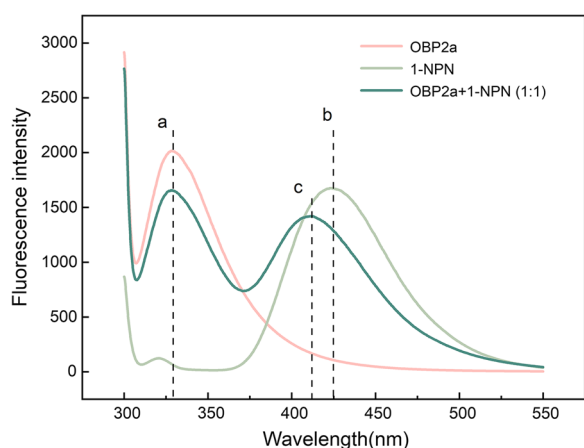
Chang *et al. Environmental Sciences Europe*   (2023) 35:44

Page 6 of 12

Fig. 1 Fluorescence spectra of OBP2a (pink line), 1-NPN (light green line) and OBP2a/1-NPN mixture (2 μmol/L:2 μmol/L) (dark green line)

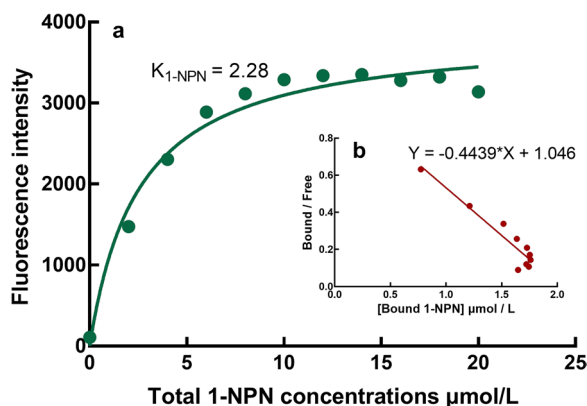**Fig. 2** Binding curve and Scatchard plot (embedded plot) of the fluorescent probe 1-NPN with OBP2a

saturation at 12 μmol/L. The binding constants of 1-NPN, 1-AMA and ANS were determined to be 2.28, 14.76, 34.76, respectively. A lower binding constant reflects a stronger affinity between OBP2a and fluorescence probe. Thus, 1-NPN was selected for assays on the binding of OBP2a to candidate odorants (Fig. 2).

Binding properties of OBP2a to 14 odorants

The competitive binding curves and dissociation constants (K_i) of the 14 odorants with OBP2a are shown in Fig. 3 and Table 2, respectively. Good reproductivity for the binding of OBP2a and odorants were observed (relative standard deviations < 10%). A smaller K_i indicates a stronger binding affinity between OBP2a and the corresponding odorant. As indicated, OBP2a has a broad binding capacity for odorants, with dissociation constants for the 14 odorants ranged from 29.91 μmol/L to 63.06 μmol/L, among which 9 odorants including

DMTS, IBMP, 2-MIB and six aldehydes (hexanal, heptanal, benzaldehyde, 2-octenal, decanal and β-cyclocitral) can reduce fluorescence intensity by more than 50%. In particular, OBP2a selectively binds to aldehydes with no more than 10 carbon atoms (K_i, 29–43 μmol/L), and the strongest binding capacity of aldehydes was for 2-octenal (K_i, 29.91 μmol/L) followed by decanal (K_i, 31.59 μmol/L) and β-cyclocitral (K_i, 34.79 μmol/L), which was in consist with literature that OBP2a appears to be specific for aldehyde-based compounds [28]. In contrast, OBP2a showed weak binding to 2-MIB and IBMP with dissociation constants of 43.89 μmol/L and 48.36 μmol/L, respectively, and almost no binding activity for geosmin, DCIP, DMDS, undecanal and 2-ethyl-4-methyl-1,3-dioxolane.

Analysis of binding modes and mechanism based on molecular docking

The predicted three-dimensional structure of wild-type OBP2a is shown in Fig. 4. OBP2a adopts the typical lipocalin structure, with a brief α-helix segment near the C-terminus and a β-barrel arrangement forming a basket around a binding cavity [43]. A stable hydrophobic cavity is formed by the hydrophobic and aromatic side chains of the amino acids.

Table 3 illustrates the molecular docking results of OBP2a with 14 odorants. The docking score characterizes the free energy of the binding of OBP2a with an odorant, and a lower score indicates a stronger binding ability for the odorant. In general, the docking scores of 14 odorants ranged from − 6.61 to − 3.04. β-Cyclocitral (score value, − 6.61), benzaldehyde (score value, − 5.63) and 2-ethyl-4-methyl-1,3-dioxolane (score value, − 5.55) exhibit relative high docking scores.

The binding modes and mechanism of 14 odorants are shown in Fig. 4 and Additional file 1: Fig. S3. Arg55, Lys112 and Phe97 were the dominant residues participating in the binding of most odorants. 4 of the 14 odorants, including DCIP, DMDS, DMTS and 2-ethyl-4-methyl-1,3-dioxolane, rely on hydrophobic interactions to bind to OBP2a. The remaining 10 tested odorants can generate hydrogen bonds with amino acid residues within the hydrophobic pocket of OBP2a. To be specific, the hydroxyl groups on 2-MIB and geosmin can interact with Arg55 to generate hydrogen bonds, respectively. The oxygen atom on the IBMP branch and the formyl groups of all aldehydes interact with Lys112 to generate hydrogen bonds. In particular, except hydrophobic and hydrogen bonding interactions, aromatic ring-containing odorants, e.g., IBMP and benzaldehyde, also interact weakly with the benzene ring on the side chain of phenylalanine by pi–pi stacking interaction. IBMP, containing a
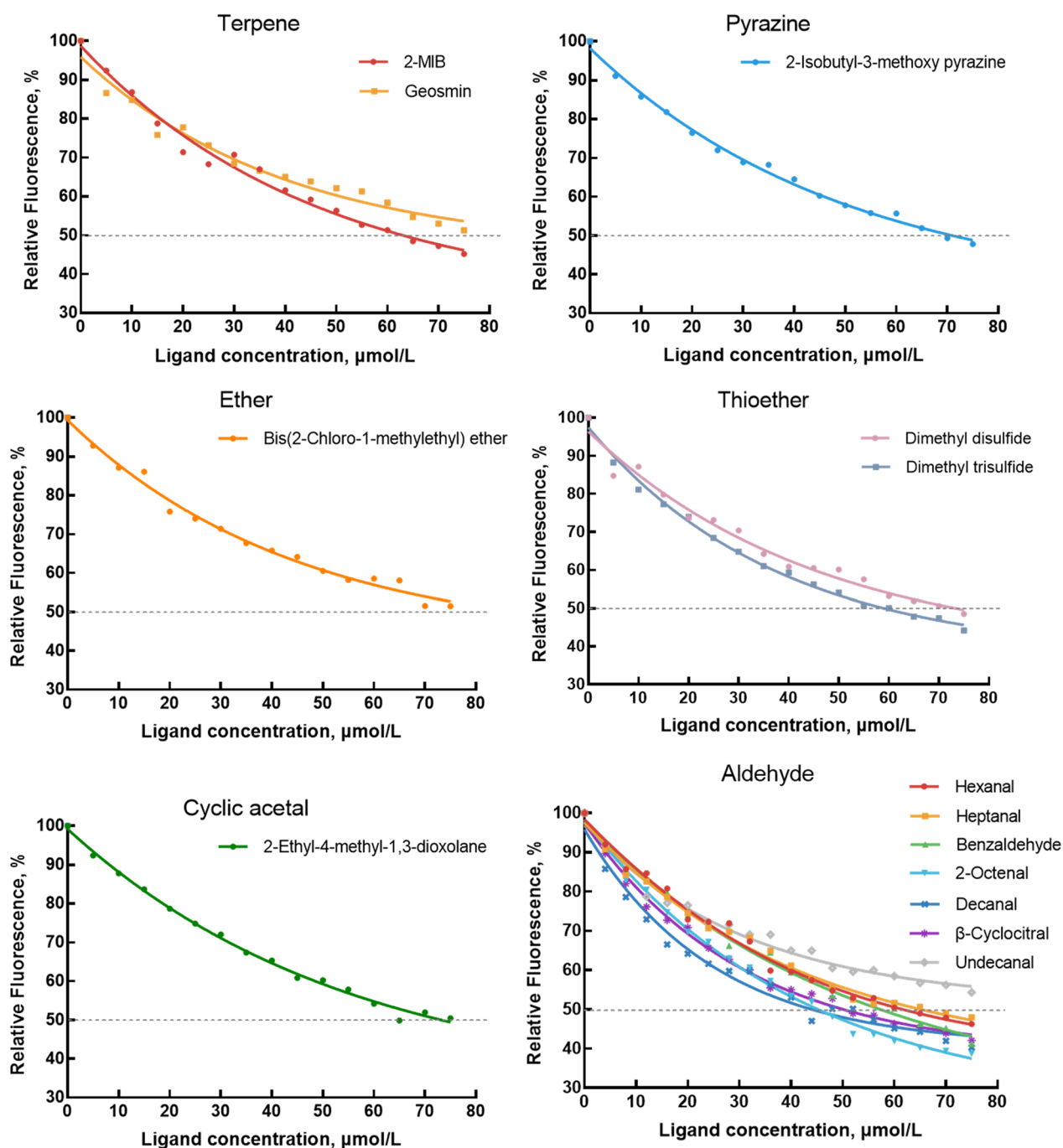
Fig. 3 Competitive binding curves of 14 odorants towards recombinant OBP2a

double nitrogen-containing six-membered heterocyclic aromatic rings, exhibits earthy/musty/sweet odor with odor threshold < 10 ng/L [11]. Molecular docking shows that IBMP can form hydrogen bonds and pi–pi stacking with Lys112 and Phe97 located deep in the binding cavity of OBP2a.

Discussion

In this study, some odorants including geosmin, 2-MIB, IBMP, DMDS, DMTS and 2E4MDL with odor threshold concentrations at low ng/L level (~ 10 ng/L) exhibit weak even no affinities. The weak binding affinities of these odorants indicates that there may be other information transfer proteins assisting odor molecules to cross the

Table 2 Binding affinities of 14 odorants to OBP2a

Odorants		IC50 [a] (µmol/L)	K_i [b] (µmol/L)	RSD [c] (%)
2-Methylisoborneol	2-MIB	63.34 ± 0.24	43.89 ± 0.17	0.36
Geosmin	GSM	90.86 ± 0.02	63.06 ± 0.01	0.02
2-Isobutyl-3-methoxy pyrazine	IBMP	71.01 ± 0.32	48.36 ± 0.22	0.44
Bis(2-chloro-1-methylethyl) ether	DCIP	81.28 ± 0.48	56.00 ± 0.38	0.59
Dimethyl disulfide	DMDS	73.90 ± 0.45	50.72 ± 0.31	0.65
Dimethyl trisulfide	DMTS	59.93 ± 0.18	41.83 ± 0.13	0.26
2-Ethyl-4-methyl-1,3-dioxolane	2E4MDL	72.74 ± 0.24	51.29 ± 0.17	0.31
Hexanal	–	61.37 ± 0.50	41.49 ± 0.39	0.81
Heptanal	–	65.71 ± 0.38	43.87 ± 0.25	0.59
Benzaldehyde	–	57.88 ± 0.21	37.25 ± 0.14	0.32
2-Octenal	–	45.35 ± 0.23	29.91 ± 0.15	0.46
Decanal	–	46.86 ± 0.20	31.59 ± 0.13	0.38
β-Cyclocitral	–	51.38 ± 3.48	34.79 ± 2.36	7.07
Undecanal	–	95.60 ± 2.40	61.05 ± 1.53	2.52

[a] The concentration of ligand halving the initial fluorescence intensity;

[b] dissociation constants between OBP2a and target odorants;

[c] the relative standard deviations (RSD) of dissociation constants for all odorants
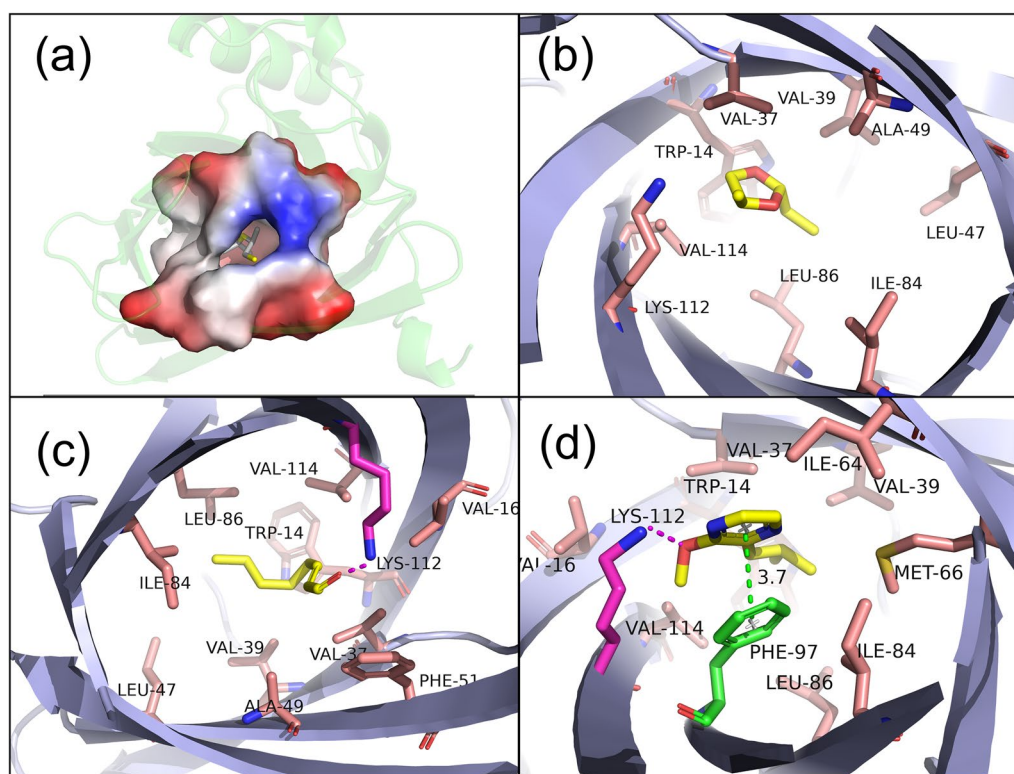

Fig. 4 Three-dimensional structure of OBP2a (**a**) and analysis of binding mechanisms of OBP2a to 2-ethyl-4-methyl-1,3-dioxolane (**b**), 2-octenal (**c**), and 2-isobutyl-3-methoxy pyrazine (**d**). Purple arrow, hydrogen bonding; green arrow, pi–pi stacking

hydrophilic barrier of the nasal mucus to reach olfactory receptors [44]. Another possible reason might be that 1-NPN and some odorants bind to OBP2a at different

active sites within the hydrophobic pocket. Interestingly, geosmin forms hydrogen bonds with the amino acid residue Arg55, while its binding affinity was lower than that

Chang *et al. Environmental Sciences Europe*   (2023) 35:44

Page 9 of 12

Table 3 Molecular docking of OBP2a with 14 odorants

Odorants		Docking score	Interaction analysis	Related amino acids
2-Methylisoborneol	2-MIB	− 3.80	H-bond	Arg 55
Geosmin	GSM	− 4.15	H-bond	Arg 55
2-Isobutyl-3-methoxy pyrazine	IBMP	− 4.87	H-bond, pi–pi stacking	Lys 112, Phe 97
Bis(2-chloro-1-methylethyl) ether	DCIP	− 3.08	–	–
Dimethyl disulfide	DMDS	− 3.04	–	–
Dimethyl trisulfide	DMTS	− 4.19	–	–
2-Ethyl-4-methyl-1,3-dioxolane	2E4MDL	− 5.55	–	–
Hexanal	–	− 3.92	H-bond	Lys 112
Heptanal	–	− 4.36	H-bond	Lys 112
Benzaldehyde	–	− 5.63	H-bond, pi–pi stacking	Lys 112, Phe 97
2-Octenal	–	− 4.73	H-bond	Lys 112
Decanal	–	− 4.15	H-bond	Lys 112
β-Cyclocitral	–	− 6.61	H-bond	Lys 112
Undecanal	–	− 3.70	H-bond	Lys 112

of DCIP, DMDS, DMTS and 2E4MDL with only hydrophobic interactions. The microstructure of the hydrophobic inner cavity of OBP2a interacts with odorant molecules in multiple ways that strengthen or restrict the binding of odorants.

This study demonstrates that molecular docking is a useful tool to predict the binding affinity for odorants with similar compound structures and binding modes. According to Spearman correlation analysis, molecular docking scores of 14 odorants were weakly correlated with the corresponding dissociation constants (n=14, r=0.53) (Additional file 1: Fig. S4), while a higher positive correlation was observed for straight-chain aliphatic aldehydes, including hexanal, heptanal, 2-octenal, decanal and undecanal (n=5, r=0.7) (Additional file 1: Fig. S5). It was reported that Schrodinger's Glide docking module aims to predict binding patterns and make binding energy estimates based on the correct pose in the pocket, and is therefore more informative in predicting the binding affinity of substances with the same binding pattern [45]. The application of molecular docking can improve the efficiency of screening the specific binding receptor-ligand thus assisting in the development of biosensors.

The binding affinities of OBP2a to aldehydes varied significantly according to fluorescent competitive binding assays. The binding affinities for the fatty aldehydes including hexanal, heptanal, 2-octenal, decanal, and β-cyclocitral, were increased with the increase of hydrophobicity of aldehydes according to Pearson correlation analysis between dissociation constants and octanol–water partition coefficients (logK$_{ow}$) (n=5, r=− 0.66) (Additional file 1: Fig. S6). These aldehydes

mainly rely on hydrophobic and hydrogen bonding interactions with Lys112 in the protein binding pocket based on molecular docking. The addition of CH_2 groups in aldehydes increases the hydrophobicity, thus strengthening the hydrophobic interaction [46]. Specially, the stronger affinity of benzaldehyde comes from its benzene ring structure by generating pi–pi stacking with Phe97, increasing its affinity substantially compared to other aliphatic aldehydes with higher hydrophobicity. In addition, undecanal exhibits the weakest affinity. A possible explanation was that the length of the undecanal molecule might exceed the size of OBP2a binding cavity, as described by Abduragimov, A. R. et al. (2000) [47]. The trailing CH_2 group stretches in the hydrophobic cavity of the lipid transport protein as the alkyl chain lengthens, and an extremely long carbon backbone makes the molecule fold during binding or removes a portion of the odorant's structure from the protein binding cavity [47, 48].

The results of this study showed that OBP2a has a broad binding spectrum with the target odorants and binds preferentially to aldehydes, e.g., 2-octenal, decanal, β-cyclocitral, benzaldehyde, illustrating the possibility for detecting aldehydes in drinking water using OBP2a. Compared to other biomaterials, e.g., olfactory receptors, odor-binding proteins have better stability [49] and resistance [50], and are readily expressed and purified in heterologous systems [20], making them substantial advantages for the development of reproducible biosensors for the detection of odorants. Previously, various OBP-based biosensors have been developed. Lu et al. [32] developed an electrochemical impedance biosensor for the detection of benzaldehyde and docosahexaenoic

Chang *et al. Environmental Sciences Europe*   (2023) 35:44

Page 10 of 12

acid in ng/L level using OBP2a; Sankaran et al. [51] used the odor-binding protein LUSH from Drosophila to construct a quartz crystal microbalance biosensor to detect alcohol with detection limits of < 5 mg/L. A limitation of using odor-binding proteins for the development of biosensors is their limited chemical space of known peptides suitable for chemical binding. Fluorescent competitive binding assays and molecular docking could assess the binding affinity and mechanisms of odor-binding protein to specific odorant. Protein engineering could increase the ranges of molecular recognition for odorant-binding proteins. In addition, considering OBP2a has a broad spectrum with odorants in drinking water, a comprehensive assessment including the capacity for analysis of the real water samples with different water matrices, accuracy and precision, selectivity and reproducibility, and anti-interference ability will be conducted for biosensors using OBP2a modified transducers for the detection of odorants.

Conclusion

According to fluorescent competitive binding assays, OBP2a has a broad binding spectrum to terpenes, pyrazines, thioethers, and aldehydes. Among the 14 target odorants, OBP2a showed good affinity for aldehydes.

Lys112 and Phe97 within the hydrophobic pocket of the protein proved to be dominant binding sites for most target odorants with high affinities. 8 odorants (IBMP and all aldehydes) interacted with Lys112 by hydrogen bonding; IBMP and benzaldehyde also produced π–π stacking with Phe97.

According to Pearson correlation analysis, hydrophobicity of aldehydes affects significantly their binding affinity to OBP2a.

Supplementary Information

The online version contains supplementary material available at https://doi.org/10.1186/s12302-023-00746-z.

Additional file 1: Table S1. The Catalogue number and brand names of all standards. **Figure S1.** SDS-PAGE analysis of recombinant OBP2a. **Figure S2.** Fluorescence spectra **a**, **c** of OBP2a, fluorescence probes and OBP2a/fluorescence probe mixture and binding curves and Scatchard plots **b**, **d** of fluorescent probes with OBP2a. **Figure S3.** Analysis of the binding patterns of 11 odorants with OBP2a. **Figure S4.** Spearman correlation analysis of docking scores and IC_{50}. **Figure S5.** Relation of docking score with IC_{50} and dissociation constants of straight-chain aliphatic aldehydes. **Figure S6.** Relation of dissociation constants with molecular weight and octanol–water partition coefficient of aldehydes.

Author details
[1]Key Laboratory of Urban Stormwater System and Water Environment, Ministry of Education, Beijing University of Civil Engineering and Architecture, Beijing 100044, China. [2]National Engineering Research Center of Industrial Wastewater Detoxication and Resource Recovery, Research Center for Eco-Environmental Sciences, Chinese Academy of Sciences, Beijing 100085, China. [3]Key Laboratory of Drinking Water Science and Technology, Research Center for Eco-Environmental Sciences, Chinese Academy of Sciences, Beijing 100085, China. [4]University of Chinese Academy of Sciences, Beijing 100049, China. [5]Yancheng Institute of Technology, Yancheng 224051, Jiangsu Province, China. [6]Beijing Waterworks Group Co., Ltd., Beijing, China.

References

1. Yang M, Yu J, Li Z, Guo Z, Burch M, Lin TF (2008) Taihu Lake not to blame for Wuxi's woes. Science 319:158
2. Watson S (2004) Aquatic taste and odor: a primary signal of drinking-water integrity. J Toxicol Environ Health A 67:1779–1795
3. Wang C, An W, Guo Q, Jia Z, Wang Q, Yu J, Yang M (2020) Assessing the hidden social risk caused by odor in drinking water through population behavioral responses using economic burden. Water Res 172:115507
4. Wang C, Yu J, Chen Y, Dong Y, Su M, Dong H, Wang Z, Zhang D, Yang M (2022) Co-occurrence of odor-causing dioxanes and dioxolanes with bis(2-chloro-1-methylethyl) ether in Huangpu River source water and fates in O3-BAC process. J Hazard Mater 430:128435
5. Wang C, Gallagher DL, Dietrich AM, Su M, Wang Q, Guo Q, Zhang J, An W, Yu J, Yang M (2021) Data analytics determines co-occurrence of odorants in raw water and evaluates drinking water treatment removal strategies. Environ Sci Technol 55:16770–16782
6. Zhang XJ, Chen C, Ding JQ, Hou A, Li Y, Niu ZB, Su XY, Xu YJ, Laws EA (2010) The 2007 water crisis in Wuxi, China: analysis of the origin. J Hazard Mater 182:130–135
7. Dou M, Wang Y, Li C (2014) Oil leak contaminates tap water: a view of drinking water security crisis in China. Environ Earth Sci 72:4219–4221

8. Sun D, Yu J, Yang M, An W, Zhao Y, Lu N, Yuan S, Zhang D (2013) Occurrence of odor problems in drinking water of major cities across China. Front Environ Sci Eng 8:411–416

9. Wang C, Yu J, Guo Q, Sun D, Su M, An W, Zhang Y, Yang M (2019) Occurrence of swampy/septic odor and possible odorants in source and finished drinking water of major cities across China. Environ Pollut 249:305–310

10. Juttner F, Watson SB (2007) Biochemical and ecological control of geosmin and 2-methylisoborneol in source waters. Appl Environ Microbiol 73:4395–4406

11. Wang C, Yu J, Gallagher DL, Byrd J, Yao W, Wang Q, Guo Q, Dietrich AM, Yang M (2020) Pyrazines: a diverse class of earthy-musty odorants impacting drinking water quality and consumer satisfaction. Water Res 182:115971

12. Guo Q, Chen X, Yang K, Yu J, Liang F, Wang C, Yang B, Chen T, Li Z, Li X, Ding C (2023) Identification and evaluation of fishy odorants produced by four algae separated from drinking water source during low temperature period: Insight into odor characteristics and odor contribution of fishy odor-producing algae. Chemosphere 324:138328

13. Liu T, Yu J, Su M, Jia Z, Wang C, Zhang Y, Dou C, Burch M, Yang M (2019) Production and fate of fishy odorants produced by two freshwater chrysophyte species under different temperature and light conditions. Water Res 157:529–534

14. Wright E, Daurie H, Gagnon GA (2014) Development and validation of an SPE-GC-MS/MS taste and odour method for analysis in surface water. Int J Environ Anal Chem 94:1302–1316

15. Son M, Cho DG, Lim JH, Park J, Hong S, Ko HJ, Park TH (2015) Real-time monitoring of geosmin and 2-methylisoborneol, representative odor compounds in water pollution using bioelectronic nose with human-like performance. Biosens Bioelectron 74:199–206

16. Wang C, Yu J, Guo Q, Zhao Y, Cao N, Yu Z, Yang M (2019) Simultaneous quantification of fifty-one odor-causing compounds in drinking water using gas chromatography-triple quadrupole tandem mass spectrometry. J Environ Sci (China) 79:100–110

17. Semin GR, Groot JH (2013) The chemical bases of human sociality. Trends Cogn Sci 17:427–429

18. Stevenson RJ (2010) An initial evaluation of the functions of human olfaction. Chem Senses 35:3–20

19. Firestein S (2001) How the olfactory system makes sense of scents. Nature 413:211–218

20. Cave JW, Wickiser JK, Mitropoulos AN (2019) Progress in the development of olfactory-based bioelectronic chemosensors. Biosens Bioelectron 123:211–222

21. Scorsone E, Manai R, Cali K, Ricatti MJ, Farno S, Persaud K, Mucignat C (2021) Biosensor array based on ligand binding proteins for narcotics and explosives detection. Sensors Actuators B Chem. https://doi.org/10.1016/j.snb.2021.129587

22. Larisika M, Kotlowski C, Steininger C, Mastrogiacomo R, Pelosi P, Schutz S, Peteu SF, Kleber C, Reiner-Rozman C, Nowak C, Knoll W (2015) Electronic olfactory sensor based on A. mellifera odorant-binding protein 14 on a reduced graphene oxide field-effect transistor. Angew Chem Int Ed Engl 54:13245–13248

23. Son M, Kim D, Kang J, Lim JH, Lee SH, Ko HJ, Hong S, Park TH (2016) Bioelectronic nose using odorant binding protein-derived peptide and carbon nanotube field-effect transistor for the assessment of salmonella contamination in food. Anal Chem 88:11283–11287

24. Lu Y, Li H, Zhuang S, Zhang D, Zhang Q, Zhou J, Dong S, Liu Q, Wang P (2014) Olfactory biosensor using odorant-binding proteins from honeybee: ligands of floral odors and pheromones detection by electrochemical impedance. Sens Actuators, B Chem 193:420–427

25. Di Pietrantonio F, Cannata D, Benetti M, Verona E, Varriale A, Staiano M, D'Auria S (2013) Detection of odorant molecules via surface acoustic wave biosensor array based on odorant-binding proteins. Biosens Bioelectron 41:328–334

26. Lu Y, Yao Y, Zhang Q, Zhang D, Zhuang S, Li H, Liu Q (2015) Olfactory biosensor for insect semiochemicals analysis by impedance sensing of odorant-binding proteins on interdigitated electrodes. Biosens Bioelectron 67:662–669

27. Manai R, Scorsone E, Rousseau L, Ghassemi F, Possas Abreu M, Lissorgues G, Tremillon N, Ginisty H, Arnault JC, Tuccori E, Bernabei M, Cali K, Persaud

KC, Bergonzo P (2014) Grafting odorant binding proteins on diamond bio-MEMS. Biosens Bioelectron 60:311–317

28. Tcatchoff L, Nespoulous C, Pernollet JC, Briand L (2006) A single lysyl residue defines the binding specificity of a human odorant-binding protein for aldehydes. FEBS Lett 580:2102–2108

29. Schiefner A, Freier R, Eichinger A, Skerra A (2015) Crystal structure of the human odorant binding protein, OBPIIa. Proteins 83:1180–1184

30. Vincent F, Spinelli S, Ramoni R, Grolli S, Pelosi P, Cambillau C, Tegoni M (2000) Complexes of porcine odorant binding protein with odorant molecules belonging to different chemical classes. J Mol Biol 300:127–139

31. Charlier L, Cabrol-Bass D, Golebiowski J (2009) How does human odorant binding protein bind odorants? The case of aldehydes studied by molecular dynamics. C R Chim 12:905–910

32. Lu Y, Zhang D, Zhang Q, Huang Y, Luo S, Yao Y, Li S, Liu Q (2016) Impedance spectroscopy analysis of human odorant binding proteins immobilized on nanopore arrays for biochemical detection. Biosens Bioelectron 79:251–257

33. Zhang Q, Li Z, Chen D, Wu S, Wang H, Li Y, Lei Z (2022) The molecular identification, odor binding characterization, and immunolocalization of odorant-binding proteins in Liriomyza trifolii. Pestic Biochem Physiol 181:105016

34. Protein Data Bank. http://www.rcsb.org. Accessed 05 Jan 2023.

35. Alshehri B, Vijayakumar R, Senthilkumar S, Ismail A, Abdelhadi A, Choudhary RK, Albenasy KS, Banawas S, Alaidarous MA, Manikandan P (2022) Molecular target prediction and docking of anti-thrombosis compounds and its activation on tissue-plasminogen activator to treat stroke. J King Saud Univ Sci. https://doi.org/10.1016/j.jksus.2021.101732

36. PubChem online database. https://pubchem.ncbi.nlm.nih.gov/. Accessed 05 Jan 2023.

37. Hussein HA, Borrel A, Geneix C, Petitjean M, Regad L, Camproux AC (2015) PockDrug-Server: a new web server for predicting pocket druggability on holo and apo proteins. Nucleic Acids Res 43:W436-442

38. Harder E, Damm W, Maple J, Wu C, Reboul M, Xiang JY, Wang L, Lupyan D, Dahlgren MK, Knight JL, Kaus JW, Cerutti DS, Krilov G, Jorgensen WL, Abel R, Friesner RA (2016) OPLS3: a force field providing broad coverage of drug-like small molecules and proteins. J Chem Theory Comput 12:281–296

39. Mahbub NI, Hasan MI, Rahman MH, Naznin F, Islam MZ, Moni MA (2022) Identifying molecular signatures and pathways shared between Alzheimer's and Huntington's disorders: a bioinformatics and systems biology approach. Inform Med Unlocked. https://doi.org/10.1016/j.imu.2022.100888

40. Audie J, Scarlata S (2007) A novel empirical free energy function that explains and predicts protein-protein binding affinities. Biophys Chem 129:198–211

41. Biessmann H, Andronopoulou E, Biessmann MR, Douris V, Dimitratos SD, Eliopoulos E, Guerin PM, Iatrou K, Justice RW, Krober T, Marinotti O, Tsitoura P, Woods DF, Walter MF (2010) The Anopheles gambiae odorant binding protein 1 (AgamOBP1) mediates indole recognition in the antennae of female mosquitoes. PLoS ONE 5:e9471

42. D'Onofrio C, Zaremska V, Zhu J, Knoll W, Pelosi P (2020) Ligand-binding assays with OBPs and CSPs. Methods Enzymol 642:229–258

43. Pelosi P, Knoll W (2022) Odorant-binding proteins of mammals. Biol Rev Camb Philos Soc 97:20–44

44. Briand L, Eloit C, Nespoulous C, Bezirard V, Huet JC, Henry C, Blon F, Trotier D, Pernollet JC (2002) Evidence of an odorant-binding protein in the human olfactory mucus: location, structural characterization, and odorant-binding properties. Biochemistry 41:7241–7252

45. Pagadala NS, Syed K, Tuszynski J (2017) Software for molecular docking: a review. Biophys Rev 9:91–102

46. Tucker RM, Mattes RD, Running CA (2014) Mechanisms and effects of "fat taste" in humans. BioFactors 40:313–326

47. Abduragimov AR, Gasymov OK, Yusifov TN, Glasgow BJ (2000) Functional cavity dimensions of tear lipocalin. Curr Eye Res 21:824–832

48. Lu Y, Huang Y, Li S, Zhang Q, Wu J, Xiong Z, Xiong L, Wan Q, Liu Q (2017) Fat taste detection with odorant-binding proteins (OBPs) on screen-printed electrodes modified by reduced graphene oxide. Sens Actuators B Chem 252:973–982

49. Paolini S, Tanfani F, Fini C, Bertoli E, Paolo P (1999) Porcine odorant-binding protein: structural stability and ligand affinities measured by

　　　fourier-transform infrared spectroscopy and fluorescence spectroscopy. Biochim Biophys Acta 1431:179–188

50. Schwaighofer A, Kotlowski C, Araman C, Chu N, Mastrogiacomo R, Becker C, Pelosi P, Knoll W, Larisika M, Nowak C (2014) Honey bee odorant-binding protein 14: effects on thermal stability upon odorant binding revealed by FT-IR spectroscopy and CD measurements. Eur Biophys J 43:105–112

51. Sankaran S, Panigrahi S, Mallik S (2011) Odorant binding protein based biomimetic sensors for detection of alcohols associated with Salmonella contamination in packaged beef. Biosens Bioelectron 26:3103–3109

Publisher's Note

Springer Nature remains neutral with regard to jurisdictional claims in published maps and institutional affiliations.